Experiments on plasma arcs at a water–air interface

Special Collection: Non-Equilibrium Dynamics, Interfaces and Mixing in Plasmas

M. Jacobs; W. Gekelman ✉ ; P. Pribyl; Y. Qian; S. Abarzhi

Check for updates

View Online   Export Citation

01 August 2025 17:06:50

Experiments on plasma arcs at a water–air interface

View Online　　Export Citation　　CrossMark

M. Jacobs,[1] W. Gekelman,[1,a) ORCID] P. Pribyl,[1] Y. Qian,[1] and S. Abarzhi[2] ORCID

AFFILIATIONS

[1]UCLA Department of Physics and Astronomy, University of California, Berkeley, California 90095, USA
[2]Department of Physics, University of Western Australia, Perth 6009, Australia

Note: This paper is part of the Special Collection: Non-Equilibrium Dynamics, Interfaces and Mixing in Plasmas.
[a)]Author to whom correspondence should be addressed: gekelman@physics.ucla.edu

ABSTRACT

An exploding water plasma experiment at UCLA investigated the expansion and morphology of a fireball with and without an external magnetic field. Diagnostics include photographs and movies (which may be downloaded) acquired with a framing camera, magnetic probes, and visible light spectra. The expansion and internal magnetic fields are very different from the unmagnetized case when a magnetic field of order 300G is applied along the expansion axis. Visible light spectra are brighter and additional lines are seen in the presence of the magnetic field. The experiment can serve as a platform for studies of interfacial mixing and possibly shed light on very different processes such as laser target physics.

I. INTRODUCTION

Ball lightnings have been observed for nearly two centuries. A historical treatment, numerous observations, and theories are described in a book by Stenoff.[1] They last for up to tens of seconds, have been reported to pass through glass windows, and are precursors to lightning strikes. Their long lives and mysterious behavior have yet to be explained, and although similar objects have been created in laboratories,[2] there are no definitive experiments or accepted theories. Often ball lightnings are formed in concert with lightning strikes. There is speculation that plasmoids[3] (free standing discharges with self-consistent electric and magnetic fields) formed in the twisted currents of lightning strikes become ball lightning. Interest in these objects has generated many experiments involving high voltage atmospheric discharges. In experiments, such as this one, bright long-lived plumes develop and rise into the air. Although motivated by ball lightning, the experiment described here does not produce one. Instead a number of interesting and complex phenomena worthy of study are catalogued here. This is not the first study of a discharge across a liquid–air interface. However, to the best of our knowledge, we are the first to measure magnetic fields associated with the plasma fireball and studied the difference between the discharge with and without the presence of an external magnetic field.

Over the past two decades, a number of papers have described glow discharges produced above aqueous electrolyte solutions. In 2002, Egorov and Stepanov[4] in Russia discovered that when a high current spark is emitted from a wet cathode protruding from the surface of an anodic electrolyte solution, a luminous plasmoid forms and remains glowing for as long as 1 s. They hypothesized that the long life of a plasmoid was due to the formation of stable clusters consisting of two hydrated ions of opposite charge and water molecules. Further investigations by the same group[5] estimated the temperature of the "cloud of warm damp air" to be ∼300 K from the rate of increase in the buoyant mass. They determined that the color of light emission is dependent on the cathode material and salts used in the electrolyte and established that the plasmoid is surrounded by a negatively charged skin.

A few years later, a group in Japan led by Tanabe reported the time dependence of visible emission spectra[6] in such an experiment. They postulated that a cascading energy transfer process from higher energy atomic and ionic emission to lower energy molecular-like emission is a possible reason for the long lifetime observed. This group also identified the three sequential processes involved in the evolution of the phenomenon.[7]

Kuleshov and collaborators in Ukraine studied a similar experimental setup and proposed a model in which a plasma column in the

aqueous solution is generated from the electrical discharge's shock wave.[8,9]

Additional diagnostics were performed by a group in Germany in 2008, including laser deflection measurements, calorimetric measurements, and electric probes.[10,11] Their work indicated that the plasmoid consists of a hot core surrounded by cool shell, possessing an electron temperature (from various atomic emissions) of $2000 - 5000\,K$ while the temperature of the neutral particles can exceed $1300\,K$. Spectral measurements of Stark broadening indicated decreasing electron densities on the order of $10^{20}-10^{22}\,m^{-3}$ in the initial (formation) phase. They also propose that chemiluminescence reactions between dissociation products of water and dissolved calcium are a source for the emission of visible radiation in the autonomous phase.

An experiment in the U.S. has shown that air is excluded from the plasma (no oxygen or nitrogen lines seen spectroscopically)[12] and Mach 4–8 shock front speeds due to the discharge pulse have been measured.[13] Schlieren photography revealed that the plasmoid possesses a fairly uniform density, while turbulent mixing occurs below the ball presumably due to the passing warm plasmoid through air and convective heating from the still warm cathode.[14]

This investigation aims to complement and extend previous work. Using high speed photography as has been done in the past,[15] we examine the effect of an imposed external magnetic field. Furthermore, we probe the plasmoid and anode-arc streamers with electrically floating B-dot probes which measured the magnetic field associated with the discharge at a number of spatial locations. This was done with and without a background magnetic field. Finally, we include measurements from emission spectroscopy.

II. EXPERIMENTAL SETUP

Figure 1 shows a schematic of the experimental setup, which is similar to that in previous papers.[1,3,7,11,12] The cylindrical discharge vessel is filled with tap water and a salt additive ($CUSO_4$) to make an electrolyte solution. A copper ring submerged 10 cm below the surface of the electrolyte solution serves as an anode, while a copper cathode is the central electrode. The cathode is isolated from the main body of water by a nylon tube, which can hold ~0.5 ml of the same electrolyte solution. A 600 μF capacitor bank is charged by a high voltage power supply that could go up to 20 kV. For the experiments discussed, the bank was charged to 8.5 kV. The discharge switch is a NL8900 ignitron. Its ignitor is connected to a 1200 V firing circuit, triggered by a pulse generator.

Figure 1(a) is a schematic of the water plasma setup and discharge circuitry. Figure 1(b) displays the current as a function of time for a 100 A discharge. The current is the same with or without the externally applied magnetic field. Note that the current does not actually reverse sign at 14 ms and this is a result of droop in the current transformer measurement. The current voltage trace is essentially the same with or without the background field. Figure 1(c) shows positions (not to scale) of the framing camera and mirror to allow for simultaneous top and side views of the apparatus. The camera field of view was large enough to encompass the mirror and the apparatus. The outer diameter of the vessel holding the liquid is 15 cm.

The electrolyte solution was made by adding $CuSO_4$ to tap water. An Omega CDH-7021 meter measured within $\pm 2\%$ a conductivity of 2.4 mS/cm, a TDS of 1.5 ppm, and 1.2 ppm of salt for all trials. A Pearson current monitor model 301X measured the discharge current.

The plasmoid's visible emission was recorded by a Phantom v7.3 high speed camera (exposure time 4 μs, sample rate 9900 fps, and resolution 640×480, f16). The camera recorded the images in grayscale with 14 bit resolution. Visible light emission was also monitored using a photodiode detector circuit with a sub-microsecond time response and a field of view of about 4 degrees. The camera was positioned 170 cm radially distant from the center of the electrode and 11 cm above the cathode. The photodiode was positioned 130 cm to the side and at a height of 11 cm relative to the cathode. A mirror [M_1 in Fig. 1(c)] was positioned 40 cm above the cathode and angled at 45 degrees to view the phenomena from above. The framing camera simultaneously recorded images from the two mirrors. Movies taken for various initial conditions are provided as the supplementary material. The cathode tip defines the origin of coordinates, (x, y, z) = (0, 0, 0), with the right-handed axes indicated in Fig. 1.

An external magnetic field, B_{0z}, was generated with three twenty-turn coils of American Wire Gauge (AWG) 5 copper wire, each with an average diameter of 20 cm. The coils were centered on the axis of the cathode, positioned at z = −4.3, 0, and 14.8 cm. The three coils were connected in series to a DC power supply. For the trials in which the external magnetic field was present, a current of 250 A or 125 A was switched on before the discharge to produce a constant magnetic field in time. At the higher current, the magnetic field at the origin was 300 G. Figure 2 is a photograph of the experimental setup without the coils or probes.

The applied magnetic field was not spatially uniform because of the unequal coil spacing. They could not be equally spaced, as that would interfere with the photography. The field at the origin was measured with a Gaussmeter and the 3D magnetic field calculated as shown in Fig. 3.

Three 3-axis Bdot probes were made to be electrically floating (*this is necessary as seen in downloadable movie "probe-explode.mp4"*) by connecting nine differential transmitters to their respective differential receivers via fiber optic cables (circuit diagram in Fig. 3). The most useful data were acquired at heights of z = 0.5 cm and z = 5.5 cm. The fluctuating magnetic field at z = 15 cm was a small fraction of a Gauss and not useful.

Figure 4 shows a typical light signal recorded by the photodiode, in this case positioned above the water plasma and aimed transversely through it. Unlike the current, the light differs when the external field is on. The light is intense for a longer time when the magnetic field is present, and there are larger fluctuations for the first 20 ms. These are reflected in the fast frame photography in the shot-to-shot variation in space and time of the spatial patterns associated with the discharge.

III. STRUCTURES IN VISIBLE LIGHT

The framing camera recorded fascinating structures which differ greatly with or without the applied magnetic field. There are provided in a supplementary material [Fig. 5 (multimedia view)]. The trunk of the plasma in contact with the solution is clearly seen to be spinning in the movie when the magnetic field is on. The structures are not reproducible from shot to shot but their general features are very similar in a given circumstance (e.g., applied magnetic field strength or bank voltage). Four frames showing the expanding plasma with and without the applied field are shown in Fig. 5. When the field is present, the
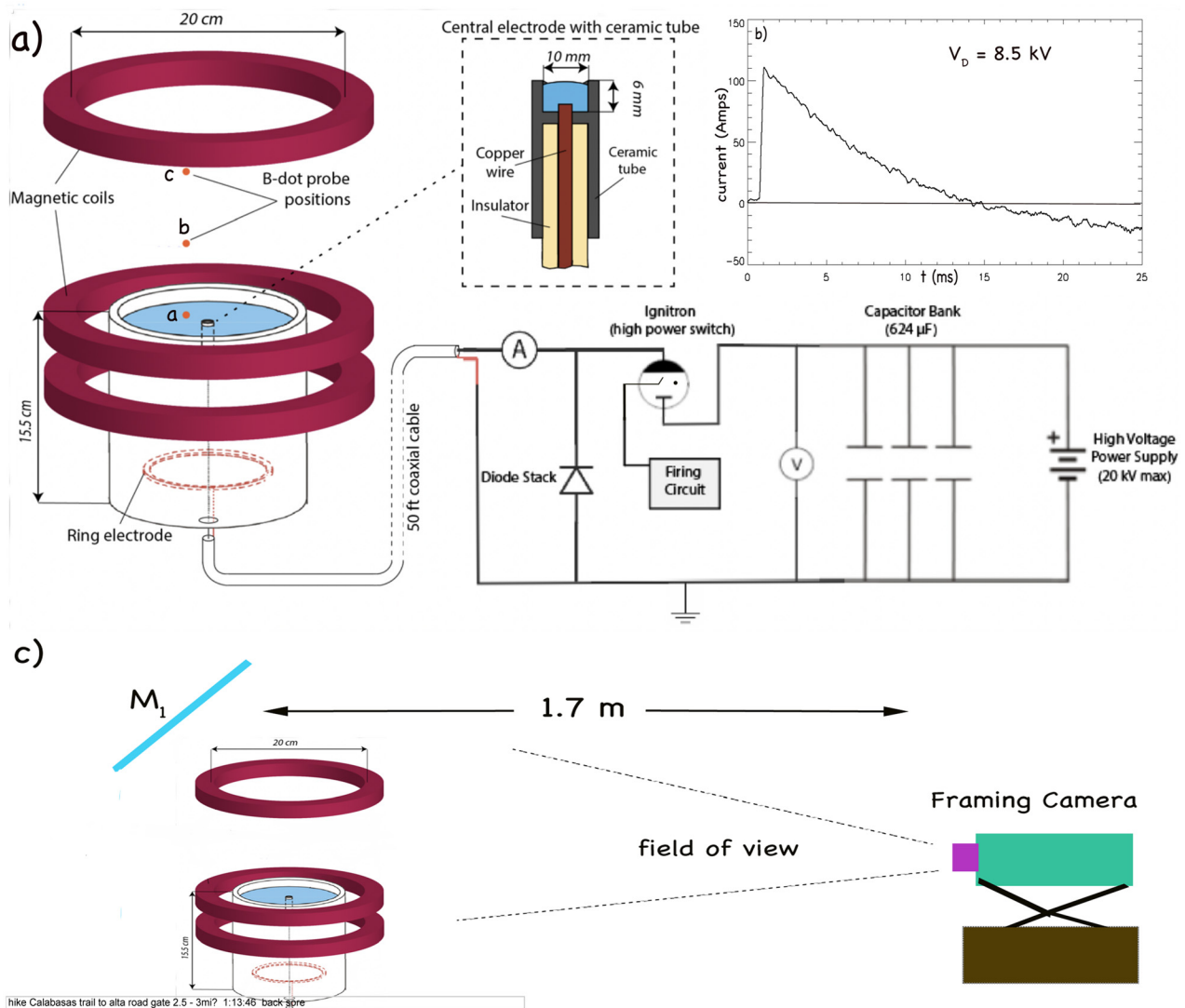
FIG. 1. Experimental setup.

structure, presumably the plasma, has risen 4.6 cm above the liquid in 300 μs for a velocity of $v_z = 1.2 \times 10^4$ cm/s. When the field is present, the column is 1.7 times higher. The column has risen to 38 cm at $t = 25.0$ ms in the unmagnetized case. The vertical velocity at that time has slowed to $v_z = 1.5 \times 10^3$ cm/s. Not visible in the still images is the rotation of the bottom of the column in the magnetized case. The plasma rotates about the point "α" in Fig. 5(c). Also visible in both cases are arcs or lightning-like structures. They are more pronounced in the unmagnetized case. The morphology of the column is different in both cases. At later times, the unmagnetized column develops flute-like structures reminiscent of a Rayleigh–Taylor instability.[16] The unmagnetized column is higher and more slender. When the magnetic field is present, the light intensity remains strong near the surface of the liquid at late times and a larger cloud forms over the apparatus. Water droplets which rise during the discharge are visible as small dots in both cases.

A mirror was used to photograph the discharge from a viewpoint looking down at the surface of the liquid. The plasma rotation, when the background magnetic field is present, is obvious as shown in a second accompanying movie [Fig 6 (multimedia view)]. As the object rotates, it changes shape making it difficult to identify structures frame-by-frame. Figure 6 shows six frames with a time interval, $\delta t = 152 \mu$s between each. Two features (α,β) can be tracked in the 761 μs interval shown. Feature α rotates by approximately $d\phi = 2.36$ radians in 304 μs leading to an angular velocity, $\omega_\alpha = \frac{d\phi}{dt} = 7.75 \times 10^3$ rad/s and rotation frequency of 1.23 kHz. The second feature, β, rotates at approximately $\omega_\beta = 5.74 \times 10^3$ rad/s and a rotation frequency of 914 Hz. The features change shape frame by frame and these are estimates at best. Although the frames suggest otherwise to the eye (as seen in the supplemental movies), it is also possible that every streamer shown in Fig. 6 is a unique arc. A camera with ten times the
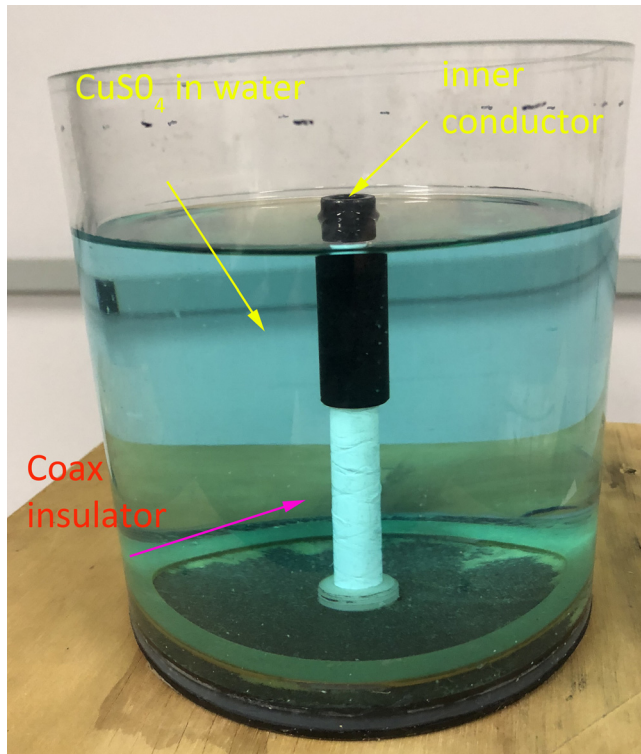
FIG. 2. Photograph of the water plasma setup without the magnetic coils. The bottom is sealed at the coax penetration with an "O ring" and nylon Swagelok connector. The outer conductor of the high voltage coaxial cable was stripped away and in addition to the cable dielectric a second layer of Teflon tape insulated the inner conductor. A Cu ring electrode on the bottom of the glass beaker was separately attached to the outer conductor of the coax, all of which was at ground potential. The water level during discharges was maintained approximately 1 mm below the plastic tube surrounding the inner conductor.

frame rate would be required to settle this unambiguously. When the background magnetic field is switched off, however, the apparent rotation disappears. Figure 7 (multimedia view) shows an arc growing in time but there is no evidence for rotation in all the frames recorded. In Figs. 5–7 the darker the image coloration, the brighter the recorded light. The color table was reversed to bring out smaller features.

IV. MAGNETIC FIELD

A set of B-dot probes were constructed to measure the changing magnetic fields associated with the currents above the liquid level. Each probe had three independent 10 turn pickup coils oriented to measure $\left(\frac{\partial \vec{B}}{\partial t}\right)$ along the three Cartesian axes. One must take care that there are no connections to ground. These can divert some or all of the current through the probe and destroy it as seen in the accompanying movie showing what happened when a Langmuir probe was connected to ground through a 1 K-Ohm resistor (it exploded). The probes were isolated electrically using an optically coupled circuit shown in Fig. 8.

The fiber transmitter circuit is a fairly standard bipolar junction transistor differential amplifier input stage as shown in panel 7(a).[17] The input signal must remain small, <100 mVp-p in this case, for the stage to remain linear. This is consistent with the small B-dot signals produced by the pickup loops. The differential current signals are coupled through fibers to a receiver stage shown in panel 7(b). The two signals may have different gains due to manufacturing variations in the fiber optics, either the transmitters, receivers, or possible flexing of the fibers. We assume that to zeroth order the variation in AC gain matches the total variation in DC gain and balance the two signals to zero the operational amplifier output using the 10 kΩ potentiometer shown in the receiver circuit. A final voltage gain of 10 converts the differential current signals to single-ended outputs for display on the scope. The input stage is powered by a battery; the first version of this circuit included a relay that could be activated by a separate fiber optic arrangement to only power the system when needed. This turned out to be unnecessary, as the battery lasts for 10 h and a simple switch to energize the circuit was adequate. Only one switch and battery were sufficient to power the nine transmitter circuits, as it turned out there was no probe-to-probe arcing. The overall voltage gain of the circuit was roughly 130 from transmitter input to receiver output, but there was enough variation between channels that each required its own calibration. The pickup probes were calibrated using a Helmholtz coil driven at several frequencies. The calibration yielded an effective area for each face.

Data were acquired with no background magnetic field and with a magnetic field of up to 300 Gauss at the surface of the liquid (Fig. 3). In the coordinate system, $z = 0$ is at the level of the water and x the radial outward distance. All data were acquired in the plane $y = 0$. At each position, four to 10 shots on three probes were recorded on 8 bit digital oscilloscopes. Signal from the first 4% of the 50 ms time traces was used to eliminate the DC offset. The data were then integrated in time. As the signal was not long enough to calculate 50 ms temporal variations, the data were smoothed over 10 ms intervals using a boxcar averaging. The smoothed signal was subtracted from the integrated data to remove low frequency trends. The final data were also smoothed to get rid of frequency fluctuations above 10 kHz. The temporal evolution of the magnetic field close to the water differs with and without the external field as shown in Fig. 9.

With no applied background magnetic field, all three components of the discharge magnetic field are present. In contrast, when the background magnetic field is switched on, the dominant field component is B_z. This indicates that a large plasma current is flowing transverse to the background magnetic field. The magnetic field varies rapidly with position. Figure 10 illustrates $\vec{B}$, 5 cm above the liquid and x = 1.5 cm.

The largest magnetic fields occur at distances of order 1 cm from the center of the system ($\mathbf{r} = 1.5, 0, 0.5$) as seen in Figs. 9 and 10. In Fig. 10(a), $B_x = 3$ G at $x = 2.5$ cm from the center. A radial current of 100 A at the height $z = 0$ would yield an azimuthal field of around 8G at this location. The axial magnetic field, B_z, is far larger when the background field is present. This suggests that there are large radial currents associated with the arcs seen in Fig. 5. Measuring the distribution of the current is a challenge and would require a great many, very small, B-dot probes making simultaneous measurements.

At this position ($x = 1$ cm), the magnetic fields 10.5 cm above the liquid are shown in Fig. 11. When the background field is present, the field is ten times smaller than the field close to the water. In Fig. 11(a), the radial component is largest but the detailed ratio between the components in three dimensions is not known. Without the background
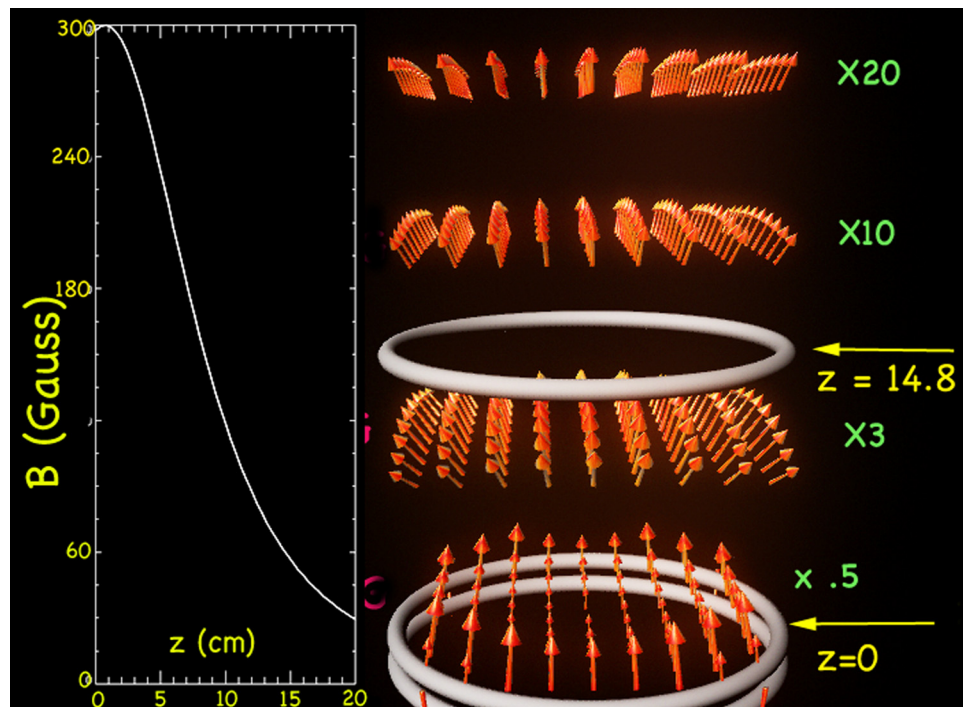
FIG. 3. Calculated magnetic field as a function of height and radius when the coil current was 250 A. Left hand side is the vertical (z) component of the magnetic field in the center of the coil. Z = 0 corresponds to the liquid level. Right hand side is three dimensional magnetic field locations at four heights. As the field drops rapidly with height, the length of the vectors was multiplied by the numbers indicated for easier viewing.

magnetic field, the changing magnetic field [Fig. 11(b)] is very small and as in Figs. 9 and 10 it has higher frequency fluctuations.

One notes that in the images taken with the fast framing camera the brightest part of the image has risen to 25.6 cm above the water at 25 ms, but is much closer to the top of the glass container at that time when the background field is present. There are large fluctuations in the first 20 ms.

The frequency spectra of the magnetic field with or without the background field are displayed in Fig. 12.
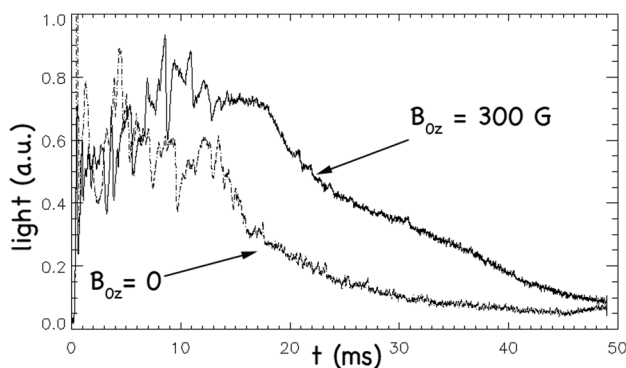

FIG. 4. Light recorded using a photodiode (arbitrary units) looking down at the water plasma. The time response of the diode was less than 1 μs.

The fluctuations are larger and have far more structure without the presence of the background field. Figure 6 indicated that with a 300G field, the rotation frequency of the spokes would be of order 1 kHz, whereas the spectra peak below 100 Hz. Note that the spectrum peaks at roughly 200 Hz with $B = 0$. Figure 5 (multimedia movie) shows that there are many more arcs when there is no background field. In addition to there being fewer arcs in the presence of the magnetic field, the arcs also disappear more quickly than in the zero-field case.

V. VISIBLE LIGHT SPECTRA

The visible light spectra were measured with an Ocean Optics Spectrometer (model HR4000). The onset of plasma current triggered a delay generator, which in turn triggered the spectrometer; spectra were acquired at several times during the evolution of the discharge, both with and without the background magnetic field. Representative spectra with several of the lines identified are shown in Fig. 13.

The spectra are highly reproducible. Lines were identified in NIST tables and from information in previously published works.[7] Stephan et al.[18] used several different electrolytes and one of them being CaCl$_2$; however, they mention that tap water contains quite a bit of Ca ions. Several Ca lines were observed in this experiment. We identify what is most likely a CuOH-CuO band at 625 nm; however, some Cu lines occur below 350 nm, below the lower cutoff of the spectrometer. Stephan as well as Versteegh et al.[10] observed CaOH bands between 550 and 650 nm. It is interesting that the spectra are more intense and include additional lines in the presence of a magnetic field.
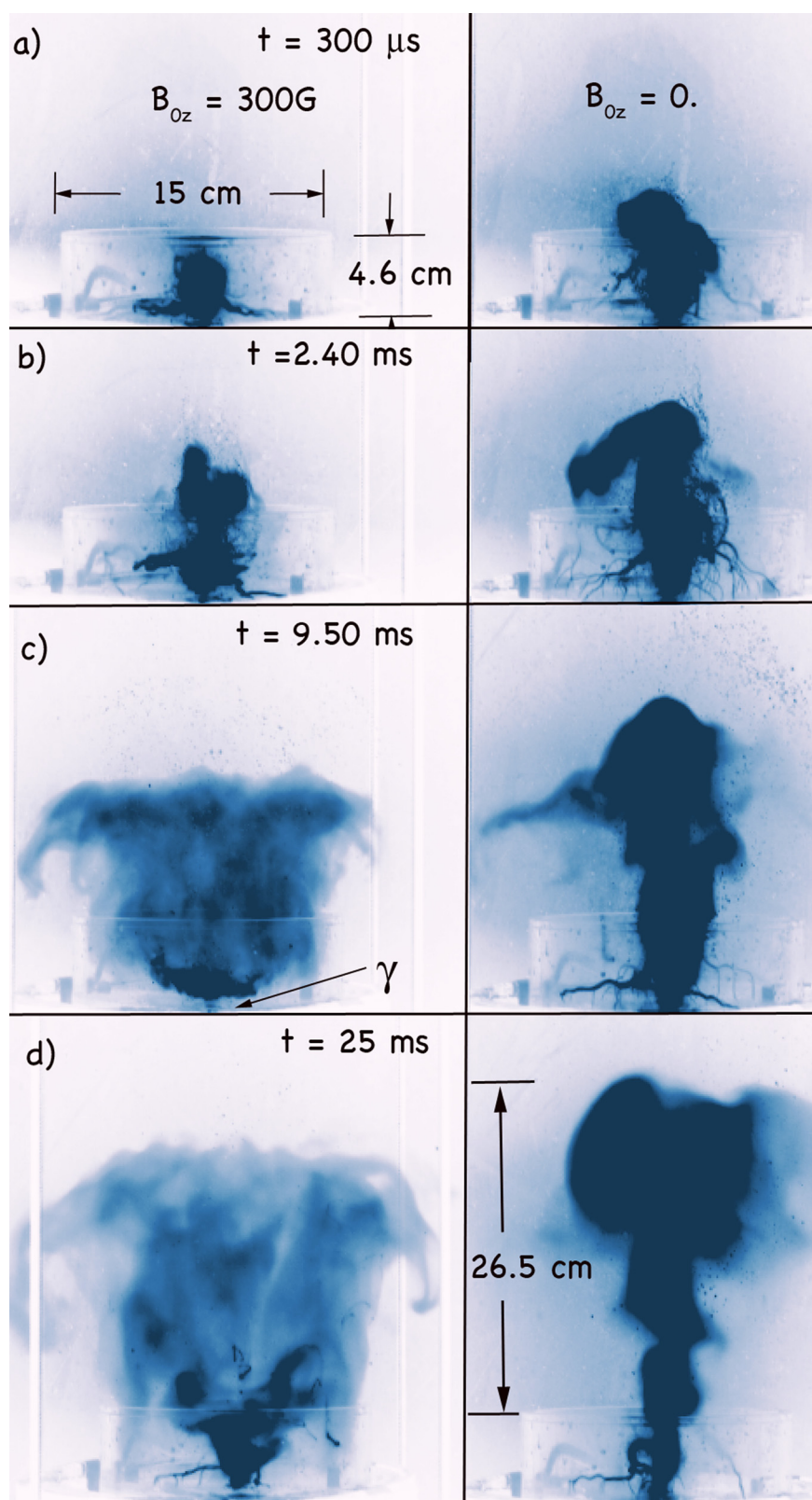
FIG. 5. Frames from the fast imaging camera at four times after the discharge is initiated at $t = 0$. The left column shows the expanding plasma with an applied magnetic field of 300G at the surface of the water. The frames on the right are taken for $B_{0z} = 0$. The times images acquired were (a) 300 μs, (b) 2.40 ms, (c) 9.5 ms, and (d) 25 ms. The surface of the liquid is at the bottom of each frame; the cathode lies slightly below it. Multimedia view: https://doi.org/10.1063/5.0040880.1
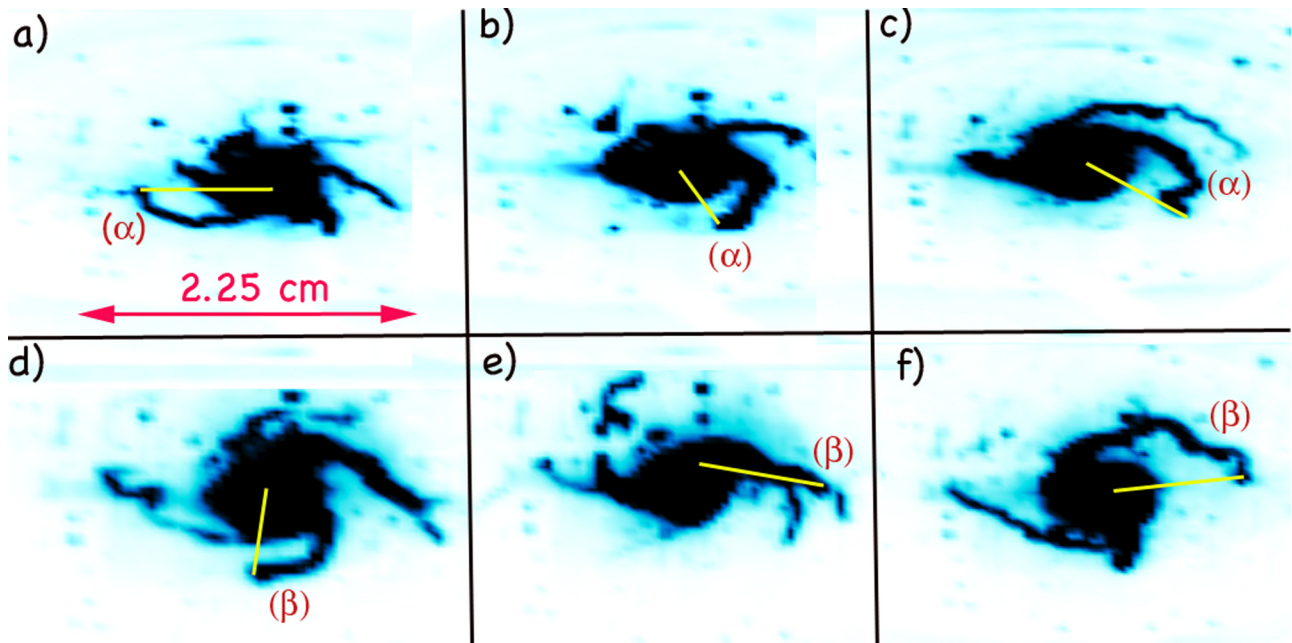
FIG. 6. Six frames from a movie (multimedia view) taken from a mirror above the plasma, which was tilted at 45 degrees. The view is nearly looking downward. The frames are at intervals of $\delta t = 152\,\mu s$ (6.57 kHz). Two features (α, β) were used to determine the rotational velocity of the spokes. Multimedia view: https://doi.org/10.1063/5.0040880.2

VI. THEORETICAL APPROACHES

The exploding water plasma experiments in this paper investigate the expansion and morphology of the fireball and detect the complex processes with the coupled hydrodynamic and electro-magnetic components. The structures observed in these experiments, such as the expanding plasma at the surface of the water in Fig. 5, appear strikingly similar to the structures developing at unstable interfaces due to the instabilities of Rayleigh–Taylor type and thus indicate the relevance of the interface dynamics to the physics of the experiments.

The instabilities of interfaces developing in multi-phase flows and the interfacial mixing they induce are a corner-stone problem of modern science, mathematics, and engineering. This challenging problem has a long history of theoretical, experimental, and numerical studies. While remarkable success has been achieved recently in the understanding of the dynamics of unstable interfaces in fluids, plasmas, and materials, at present, one has yet to develop a theory of unstable interfaces and interfacial mixing under conditions of the exploding water plasma experiments shown in Figs. 5–7.

The purposes of this section are as follows: to attract attention to the exploding water plasma experiments of the mathematicians and theoreticians working in fluids, plasmas, and materials; to emphasize the need in new theoretical studies for better understanding the
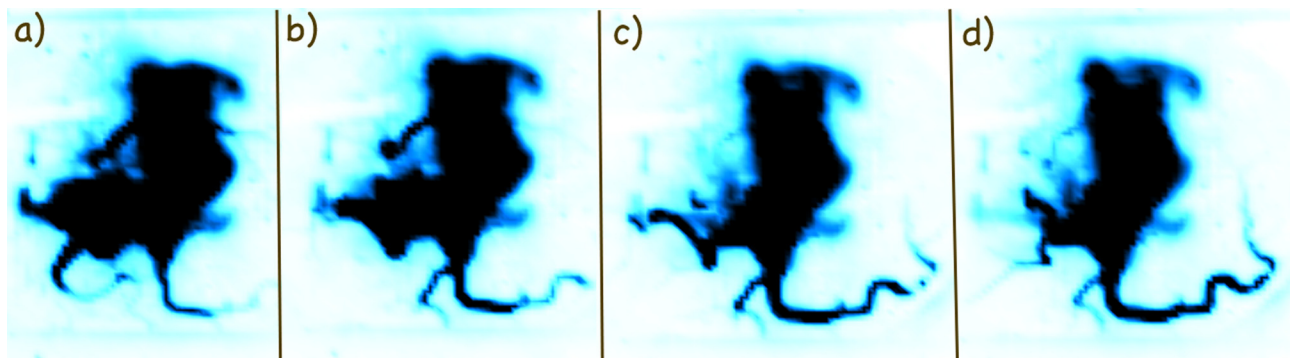

FIG. 7. Frames from a top view as in Fig. 6. Here the background magnetic field is zero and the frames are at intervals of $\delta t = 100\,\mu s$ (10 kHz). There is no evidence of rotation throughout a sequence of 256 images. Over the course of time, the arcs grow, change shape, and then vanish. The experimental sequence may be viewed in the downloadable movie. Multimedia view: https://doi.org/10.1063/5.0040880.3
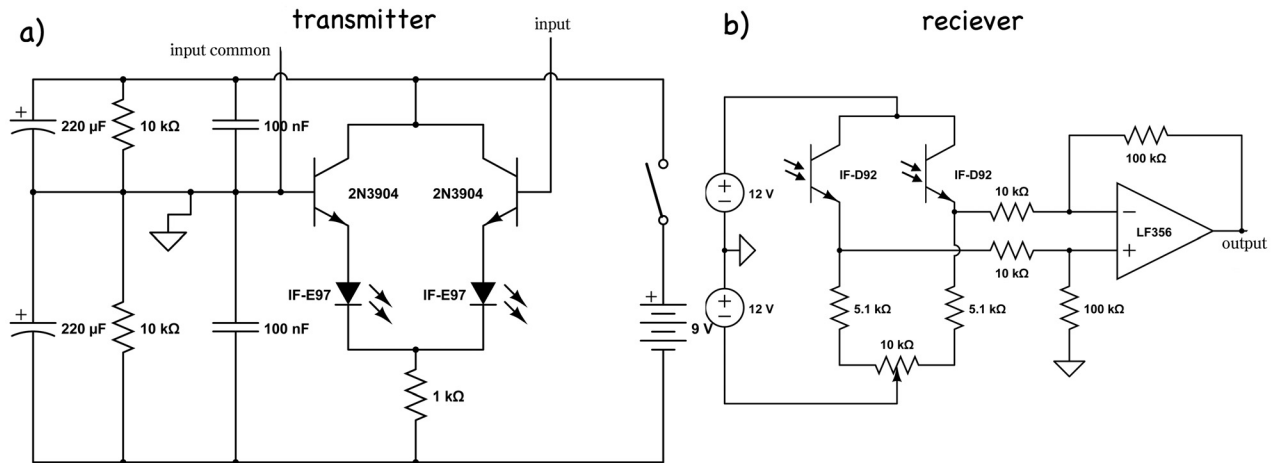
01 August 2025 17:06:50

FIG. 8. Fiber optics transmitter and receiver. Nine transmitters [panel (a), only one shown] sensitive to B-dot signals of less than 100 mV sent the differential signals through a pair of fibers to a set of differential receivers, panel (b). All transmitters were powered from the same battery.
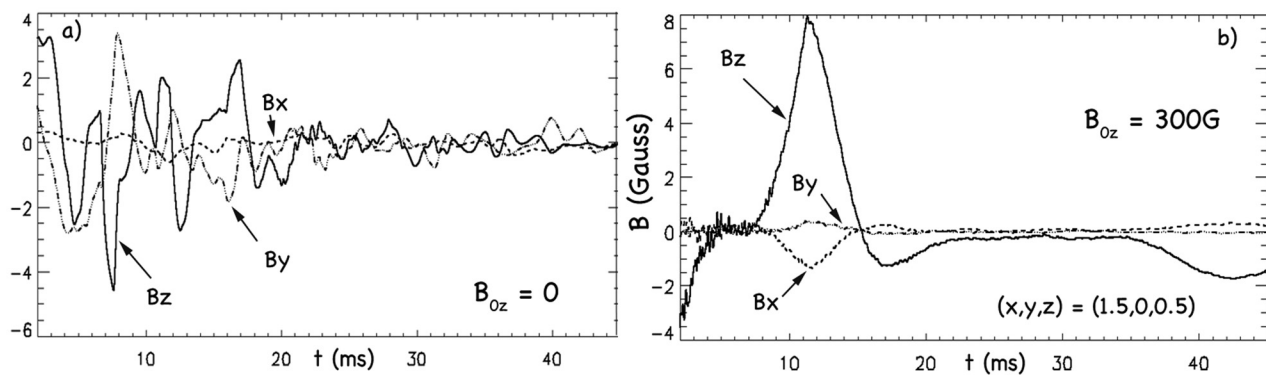

FIG. 9. Discharge magnetic field at location $(x,y,z) = (1.5,0,0.5)$ cm (5 mm above the liquid surface) when there is no background magnetic field is shown in Fig. 8(a). Figure 9(b) shows the case with 300G at the surface. The mean standard deviation of the discharge B_z is 0.8 Gauss.
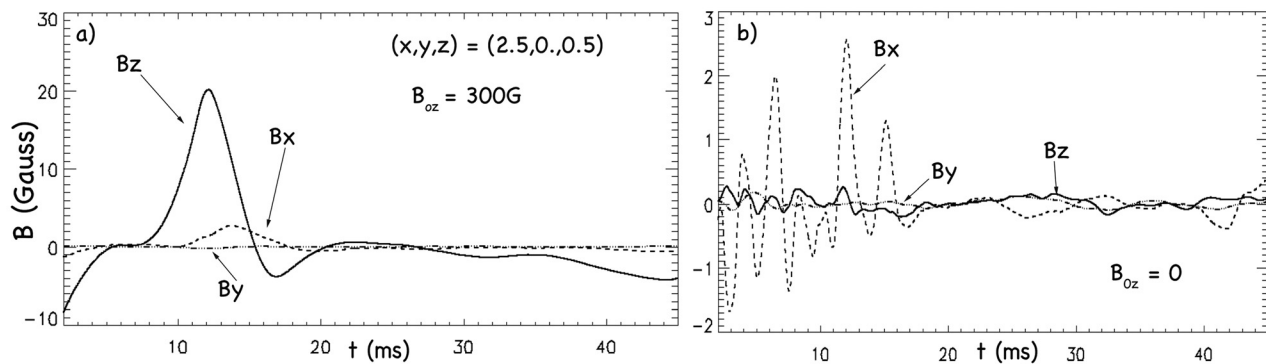

FIG. 10. Magnetic field at location $(x,y,z) = (2.5,0,0.5)$ cm. With a 300G field [Fig. 10(a)] and when there is no background magnetic field [Fig. 10(b)].
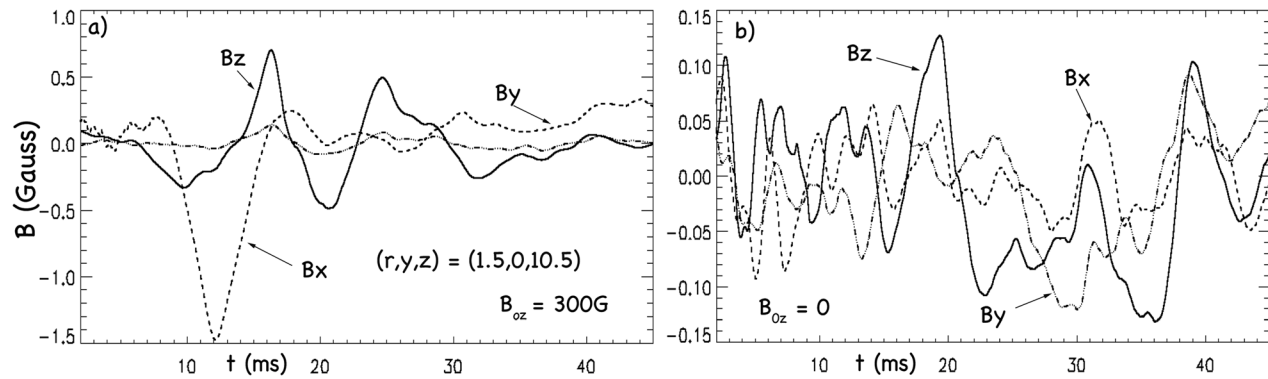
01 August 2025 17:06:50

FIG. 11. Magnetic field 10.5 cm above the liquid. (a) Background field is 300 G. (b) There is no background magnetic field.

experimental observations, particularly, the effect of the magnetic field on the structures of the expanding plasmas at the water surface; and to provide some "thought food" to experiments in high and in low energy density plasmas.

Interfaces and mixing govern a broad range of plasma processes in high and in low energy density regimes. Examples include formation of hot spot in inertial confinement fusion, thermonuclear flashes in type-Ia supernova, coronal mass ejections in the Solar flares, plasma thrusters, and plasma discharges formed in and interfacing with liquids.[19–25] In theories describing these processes, the interface is usually viewed as a phase boundary, and the phases are broadly defined. These can be the distinct kinds of matter and the same kind of matter with distinct thermo-dynamic and/or electro-magnetic properties. The matter(s) may also experience phase transition(s), be out of thermodynamic equilibrium, and have non-diffusive transports across the interface.[19–22,30,31] In the experiments presented in the paper, the phases are the expanding plasma and the water, Figs. 5–7.

For neutral plasmas (fluids), two types of phase boundaries are usually considered—a front (with zero mass transport across it) and an interface (through which mass can be transported).[28,29] Fronts are usually destabilized by accelerations, leading to Rayleigh–Taylor (RT) instabilities.[20,21,26–28] The RT dynamics is essentially interfacial, with intense motions near the interface, with effectively no motions away from the interface, and with vortical structures appearing at the interface.[20,21,28] This interfacial character of the dynamics also holds in the presence of magnetic fields.[29,30] Moreover, RT mixing may exhibit coherence and order even at very high Reynolds numbers, thus explaining experiments.[20,21,28,31,32] For interfaces, recent theories[19,22,29,31] revealed the inertial stabilization mechanism and the new instability of the accelerated interface. In this dynamics, vortical
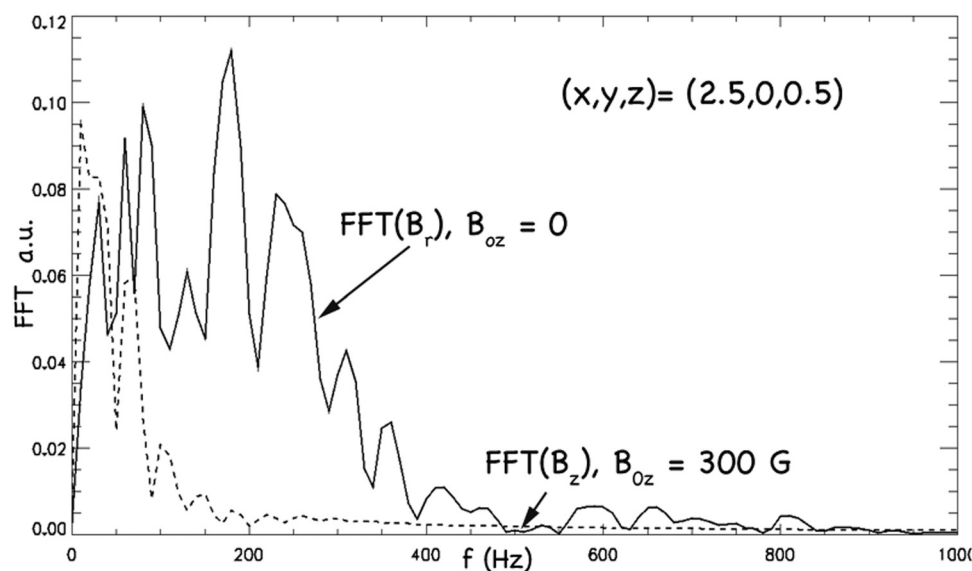

FIG. 12. Frequency spectra of the largest component of the magnetic field for the case of Fig. 10. The spectra of B_r without the background magnetic field are shown as a solid line and that of B_z as a dashed line. Spectra up to 1 kHz are shown and the signal above this is very small. The signal was digitized at 200 kHz.
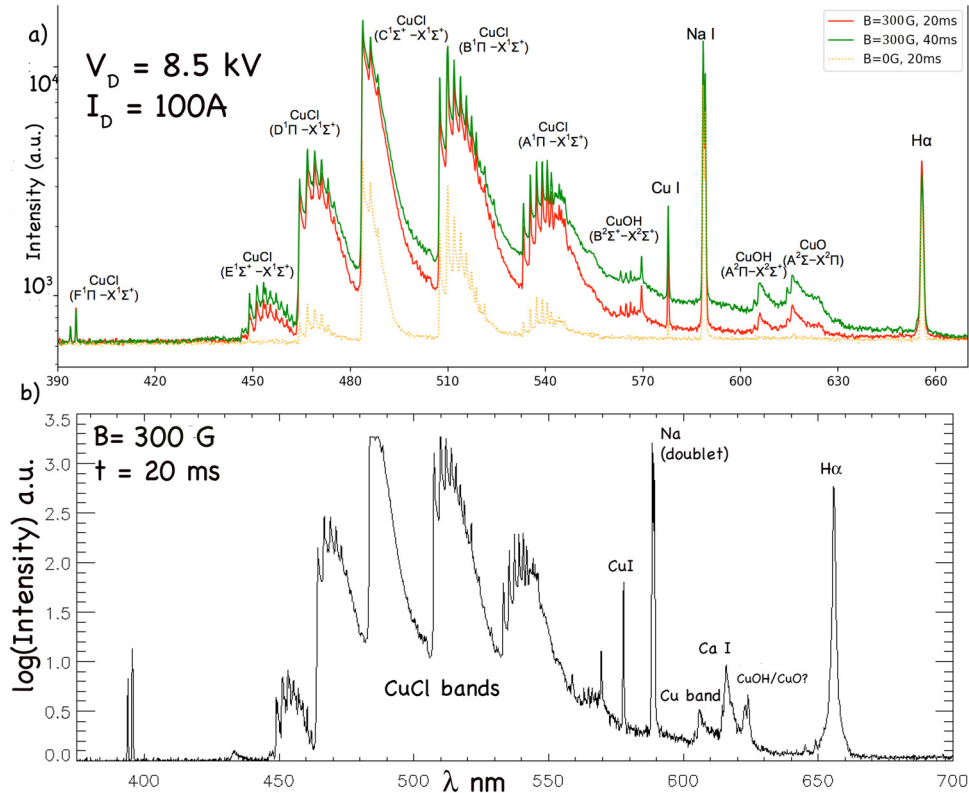
FIG. 13. (a) Visible lines and bands as a function of time on a linear scale (units are arbitrary). Each spectrum was recorded on a separate shot. The spectrum drawn in yellow is for the case of no background magnetic field. (b) Spectra at t = 20 ms, when the 300G background field is present, displayed on a log scale to bring out the smaller amplitude lines. The response time of the Ocean Optics spectrometer is as short as 1 μs, although for these experiments the integration time was typically set to 20 ms.

structures may appear only in the bulk; they are energetic in nature and are caused by energy imbalance at the interface.[19,24,29] These theoretical approaches can be further expanded to account for electromagnetic effects and explain the difference in the expansion and morphology of the fireball with and without the magnetic field, observed in the experiments, Figs. 5–7. We address these studies to the future.

We also note that in high energy density plasmas, such as inertial confinement fusion and supernovae, the good grip and control on plasma hydrodynamics are in demand.[23–25] Particularly, fluid instabilities and interfacial mixing are known to be the determining factors in the hot spot formation in inertial confinement fusion and in the mechanism for energy transport and nuclear synthesis in core-collapse supernova.[23–25,28–31] Since fluid instabilities and interfacial mixing are known to have very similar behaviors in the vastly different physical regimes,[28–32] the exploding water plasma experiments presented in this paper may potentially serve as test-bed for studies of the unstable hydrodynamics and the interplay of electro-magnetic and hydrodynamic effects in plasmas, including fusion relevant conditions.[23,25,32] These experiments have high reproducibility and repeatability, are affordable, and have relatively tight control of experimental parameters and conditions. They may provide data and diagnostics for dynamics of realistic plasmas with unstable interfaces over a broad range of parameters in a well-controlled laboratory environment and thus complement the existing

approaches elaborating the means of control of plasmas flows in high and low energy density regimes.[25]

VII. SUMMARY AND CONCLUSIONS

The behavior of the plasma fireball is markedly different with or without a background magnetic field. When no field is present, the structure moves upward faster than in the magnetized case. In Fig. 5(d), it has risen 26.5 cm in 25 ms, with an approximate vertical velocity $v_z = 106$ m/s. This is very slow compared to ion or electron time scales and is attributed to hydrodynamic motion of the gas cloud (which may be partially ionized) above the liquid. The percent ionization was not measured here, but other experiments have estimated it to be low (0.1%).[14] With an externally applied magnetic field, the brightest region remains closer to the liquid and the cloud above it flattens into a cylinder with curled fingers spilling over the top [Fig. 5(c) and 5(d)]. With no field, the column is narrower and brighter throughout its volume. In either case, arcs, which resemble miniature lightning strikes, between the center of the column and liquid are present. With applied magnetic field, there are qualitatively fewer of them than in the zero field case. More noteworthy, the apparent rotation of the lightning spokes takes place when the field is present. This is visible in the movies which can be downloaded as part of this publication. The rotation estimated from the frames was of order 1 kHz, which is a much higher frequency than the fluctuations in the magnetic field

01 August 2025 17:06:50

spectra near the liquid (Fig. 12). The azimuthal rotation might suggest the presence of a radial electric field, $v_\phi = \frac{E}{B}$; however, the electron neutral collision frequency in excess of 10 GHz speaks against this. There are $\vec{J} \times \vec{B}$ forces, but they are small and estimated to be about 1 newton. Magnetic fields generated are small, tens of Gauss near the liquid; nevertheless, they are a significant fraction of the background field. The discharge magnetic field drops off rapidly with height; fluctuations are larger and seem to permeate the cloud when there is no background field. Electrons with a temperature of 0.5 eV have a gyroradius of 1.7 mm; however, the electron cyclotron frequency, a 300 G, near the surface of the liquid is 84 MHz, far less than the electron neutral collision frequency at atmospheric pressure. Because of this one would *a priori* expect the background field to play no role. The difference in visible light photographs (Fig. 5) with and without the external field, however, indicates that the magnetic field does have a significant effect. The magnetic field frequency spectra have far more structure without external magnetic field indicating that the presence of B_{0z} may suppress instabilities in the column. The presence of the magnetic field is also manifested in the visible light spectra shown in Fig. 12. The emission is much stronger in the presence of the field and grows in time although many of the spectral lines/bands are the same. It is

interesting that the field has any effect at all, as the electron-neutral collision frequency is many orders larger than the electron cyclotron frequency.

The evolution of the structures shown in Fig. 5 is clearly different with or without the presence of the magnetic field. In both cases, the brightest part of the glowing volume rises initially. In the magnetized case, the rate of rise slows to almost zero. This is exemplified in Fig. 14(a) showing boundary height as a function of time. The boundary of the brightest part of the column was determined by finding the location of a sharp gradient in the light shown in Fig. 5. When the magnetic field is present, the light was not as uniform as in the field free case and the average boundary height is calculated over the region $x = -2$ to 2 cm. Without an external magnetic field, the plasma smoothly rises to 38 cm above the surface in 25 ms ($v_z = 1.52 \times 10^3$ cm/s). In this case, shown in Fig. 14(b), the plot of ln(*height*) as a function of time continues to increase after 15 ms. With magnetic field, a similar plot of ln(*height*) is noisier, although its late time behavior may track the unmagnetized case. Figures 14(c) and 4(d) show the plumes at 25 ms. When the magnetic field is present, the cloud, presumably water vapor, above the brightest part is mushroom shaped. Interestingly, this is similar to the vortex sheet and Rayleigh–Taylor
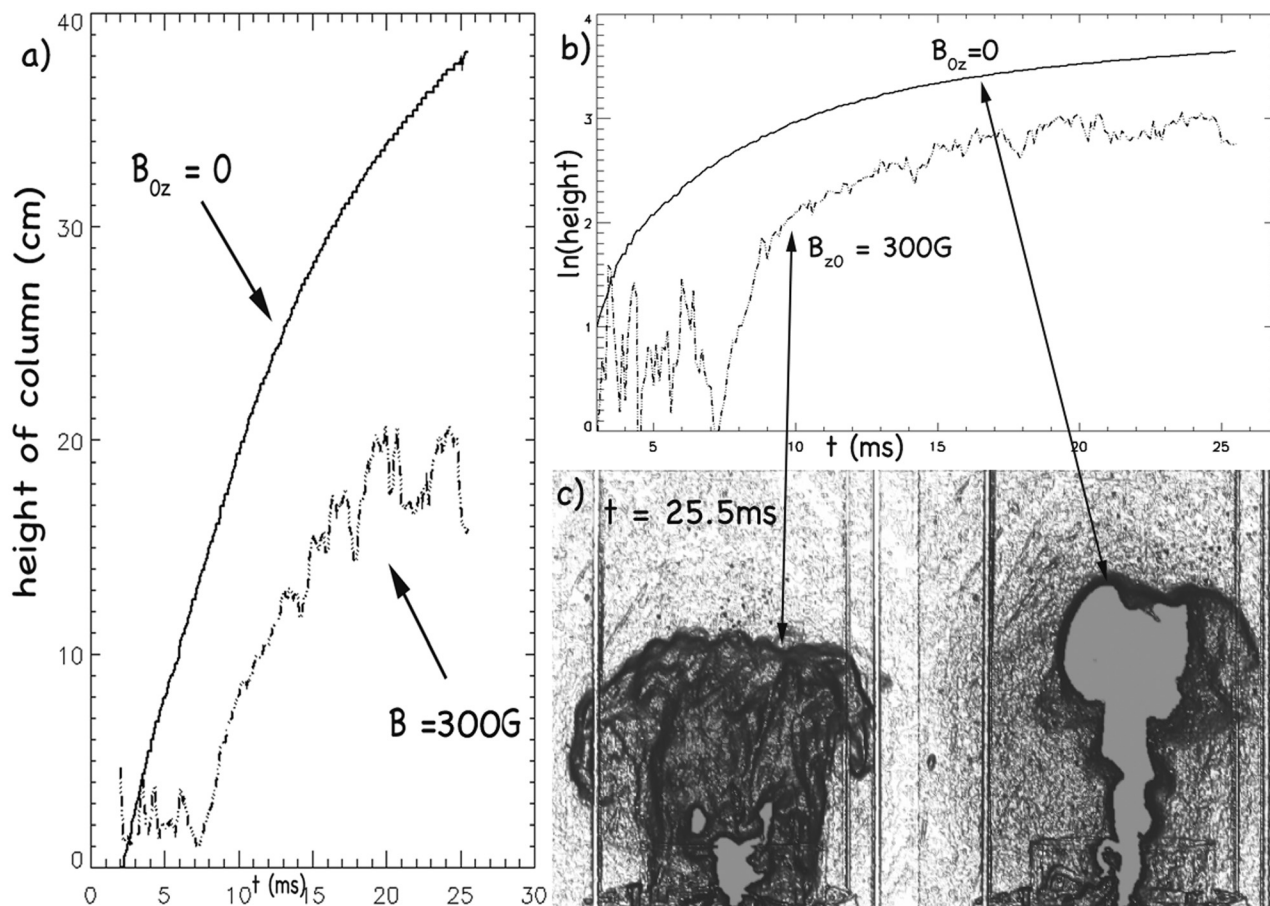

FIG. 14. (a) Height of the brightest part of the plasma plume [see Figs. 5 and 14(c)] as a function of time with and without the presence of the external magnetic field. When the height curves are plotted as a function of time on a semilog scale [Fig. 14(b)], they approach a straight line after 15 ms. Figure 14(c) shows the plumes at a late time.

unstable structures,[24–27,29] though in the simulations[29] the applied magnetic field was parallel to the interface.

The experiment suggests that detailed maps of the magnetic field should be made in the future. This experiment was a summer project and magnetic field data were acquired at only six locations and for only 4–10 shots at each position. The shot to shot variation is large and taking data with very small probes over a large grid with enough shots at each location to develop reliable statistics will be time consuming but, in our opinion, may go a long way toward deeper understanding of these phenomena. Further theoretical investigation of the underpinnings of the plume may contribute to the understanding and control of plasma flows in high and low energy density regimes.

While the experiments are relatively easy to implement within a laboratory form-factor, they unambiguously reveal complex plasma transport processes with coupled hydrodynamic and electro-magnetic components (Fig. 14). In order to better understand these complex processes, additional measurements and diagnostics are required. These may include, for instance, time and spaced resolved spectroscopy, Langmuir type probe measurements of plasma density and electron temperature, microwave interferometry, Thompson scattering (electron density and electron temperature), 3D imaging with fast framing cameras, etc. We hope that future research will address these issues. Complete understanding dictates a long term experimental and theoretical program.

The interface dynamics of the structures observed in our experiments appear very similar to the structures developing at unstable interfaces due to the instabilities of Rayleigh–Taylor type (Fig. 5). The dynamics of unstable interfaces and interfacial mixing is studied traditionally in high energy density plasmas, including the formation of hot spot in inertial confinement fusion and the mechanism for energy transport in core-collapse supernova.[24–32]

The characteristic features of our experiments are their high reproducibility, repeatability, and affordability, and the relatively tight control of experimental parameters and conditions. These features may enable the detailed study of the dynamics of realistic plasmas with unstable interfaces over a broad range of parameters in a well-controlled laboratory environment and may complement the existing approaches elaborating the means of control of plasmas flows in high and low energy density regime, including fusion and supernova.[24–32]

SUPPLEMENTARY MATERIAL

See the supplementary material for Video "probe-explore.mp4" Video of a Langmuir probe attached to ground via a resistor. When the plasma contacts it the probe explodes.

ACKNOWLEDGMENTS

DATA AVAILABILITY

The data that support the findings of this study are available from the corresponding author upon reasonable request.

REFERENCES

[1] M. Stenhoff, *Ball Lightning, an Unsolved Problem in Atmospheric Physics* (Klumwer Academic/Plenum Publishers, New York, 1999).

[2] H. Ofuruton, N. Kondo, M. Kamogawa, M. Aoki, and Y. Ohusuki, "Experimental conditions of laboratory ball lightning produced by microwave and discharge," in *Proceedings: 5th International Symposium on Ball Lightning*, ISBL97 (Daito-Insatsu Kogyo Co., 1997), Vol. 17.

[3] W. H. Bostick, "Experimental study of plasmoids," Phys. Rev. **106**, 404 (1957).

[4] A. I. Egorov and S. I. Stepanov, "Long-lived plasmoids produced in humid air as analogues of ball lightning," Tech. Phys. **47**, 1584 (2002).

[5] A. I. Egorov and S. I. Stepanov, "Properties of short-living ball lightning produced in the laboratory," Tech. Phys. **53**, 688 (2008).

[6] Y. Sakawa, K. Sugiyama, T. Tanabe, and R. More, "Fireball generation in a water discharge," Plasma Fusion Res. Rapid Commun. **1**, 039 (2006).

[7] N. Hayashi, H. Satomi, T. Kajiwara, and T. Tanabe, "General nature of luminous body transition produced by pulsed discharge on an electrolyte solution in the atmosphere," IEEJ Trans. Electr. Electron. Eng. **4**, 674 (2009).

[8] A. A. Bulgakov, B. P. Yefimov, A. N. Kuleshov, and M. O. Khorunzhiy, "Experimental investigation into spherical plasma formations," Telecommun. Radio Eng. (Engl. Transl.) **64**, 833 (2005).

[9] A. A. Bulgakov, B. P. Yefimov, E. Khutoryan, M. Khorunzhiy, and A. Kuleshov, "Excitation and observation of ball-lightning type spherical formations," in *Conference Proceedings: The 12th International Conference on Mathematical Methods in Electromagnetic Theory: MMET*08: Odesa, Ukraine, June 29−July 02* (IEEE, Piscataway, NJ, 2008).

[10] A. Versteegh, K. Berhringer, U. Fantz, G. Fussmann, B. Jüttner, and S. Noack, "Long-living plasmoids from an atmospheric water discharge," Plasma Sources Sci. Technol. **17**, 024014 (2008).

[11] S. Noack, A. Versteegh, B. Jüttner, and G. Fussmann, "Analysis of long-living plasmoids at atmospheric pressure," AIP Conf. Proc. **933**, 129 (2008).

[12] C. J. Wurden and G. Wurden, "Free-floating atmospheric pressure ball plasmas," IEEE Trans. Plasma Sci. **39**, 2078 (2011).

[13] W. L. Morgan and L. A. Rosocha, "Surface electrical discharges and plasma formation on electrolyte solutions," Chem. Phys. **398**, 255 (2012).

[14] D. M. Friday, P. B. Broughton, T. A. Lee, G. A. Schutz, J. N. Betz, and C. M. Lindsay, "Further insight into the nature of ball-lightning-like atmospheric pressure plasmoids," J. Phys. Chem A **117**(39), 9931 (2013).

[15] V. Stelmashuk and P. Hoffer, "Experimental study of a long-living plasmoid using high-speed filming," IEEE Trans. Plasma Sci. **45**, 3160 (2017).

[16] H. J. Kull, "Theory of the Rayleigh-Taylor instability," Phys. Rep. **206**, 197 (1991).

[17] See https://wiki.analog.com/university/courses/electronics/text/chapter-12 for an Analog Devices open source textbook which details the fiber transmitter circuit.

[18] K. Stephan, S. Dumas, L. Komola-Noor, and J. McMinn, "Initaion growth and plasma characterostics of 'Gatchina' water plasma," Plasma. Sources Sci. Technol. **22**, 025018 (2013).

[19] R. P. Drake, "Perspectives on high-energy-density physics," Phys Plasmas **16**, 055501 (2009).

[20] R. Betti and O. A. Hurricane, "Inertial-confinement fusion with lasers," Nat. Phys. **12**, 435 (2016).

[21] B. A. Remington, H.-S. Park, D. T. Casey, R. M. Cavallo, D. S. Clark, C. M. Huntington, C. C. Kuranz, A. R. Miles, S. R. Nagel, K. S. Raman, and V. A. Smalyuk, "Rayleigh–Taylor instabilities in high-energy density settings on the National Ignition Facility," Proc Natl Acad. Sci. U. S. A. **116**, 18233 (2019).

[22] T. C. Underwood, K. T. Loebner, V. A. Miller, and M. A. Cappelli, "Dynamic formation of stable current-driven plasma jets," Sci. Rep. **9**, 2588 (2019).

[23] T. Kaneko, K. Baba, and R. Hatakeyama, "Static gas-liquid interfacial direct current discharge plasmas using ionic liquid cathode," J Appl. Phys. **105**, 103306 (2009).

[24] S. I. Abarzhi, A. K. Bhowmick, A. Naveh, A. Pandian, N. C. Swisher, R. F. Stellingwerf, and W. D. Arnett, "Supernova, nuclear synthesis, fluid instabilities and mixing," Proc. Natl. Acad. Sci. U. S. A. **116**(37), 18184 (2019).

[25] S. I. Abarzhi, D. V. Ilyin, W. I. I. Goddard, and S. Anisimov, "Interface dynamics: New mechanisms of stabilization and destabilization and structure of flow fields," Proc. Natl. Acad. Sci. U. S. A. **116**(37), 18218 (2019).

01 August 2025 17:06:50

[26]E. E. Meshkov and S. I. Abarzhi, "On Rayleigh-Taylor interfacial mixing," Fluid Dyn. Res. **51**, 065502 (2019).

[27]N. C. Swisher, C. Kuranz, W. D. Arnettt, O. Hurricane, H. Robey, B. A. Remington, and S. I. Abarzhi, "Rayleigh-Taylor mixing in supernova experiments," Phys Plasmas **22**, 102707 (2015).

[28]H. F. Robey, Y. Zhou, A. C. Buckingham, P. Keiter, B. A. Remington, and R. P. Drake, "The time scale for the transition to turbulence in a high Reynolds number, accelerated flow," Phys Plasmas **10**, 614 (2003).

[29]C. Matsuoka, "Motion of non-uniform double current-vortex sheets in magnetohydrodynamic flows," Phys. Scr. **91**, 034005 (2016).

[30]C. Matsuoka, K. Nishihara, and T. Sano, "Nonlinear interfacial motion in magnetohydrodynamic flows," High Energy Density Phys. **31**, 19–23 (2019).

[31]D. V. Ilyin, Y. Fukumoto, W. A. Goddard III, and S. I. Abarzhi, "Analysis of dynamics, stability and flow fields' structure of an accelerated hydrodynamic discontinuity with interfacial mass flux by a general matrix method," Phys. Plasmas **25**, 112105 (2018).

[32]O. A. Hurricane, D. A. Callahan, D. T. Casey, E. L. Dewald, T. R. Dittrich, T. Döppner, M. B. Garcia, D. E. Hinkel, L. F. B. Hopkins, P. Kervin *et al.*, "The high-foot implosion campaign on the National Ignition Facility," Phys Plasmas **21**, 056314 (2004).

01 August 2025 17:06:50